Available online at www.sciencedirect.com
SCIENCE DIRECT
Journal of Organometallic Chemistry 691 (2006) 371–379
Journal of Organometallic Chemistry
www.elsevier.com/locate/jorganchem

# Ligand substitution in the heterometallic cluster $Cp^*IrOs_3(\mu\text{-}H)_2(CO)_{10}$

Padmamalini Srinivasan, Weng Kee Leong *

*Department of Chemistry, National University of Singapore, Kent Ridge, Singapore 119260, Singapore*

Received 18 August 2005; received in revised form 5 September 2005; accepted 6 September 2005
Available online 27 October 2005

**Abstract**

The reactions of the heterometallic cluster $Cp^*IrOs_3(\mu\text{-}H)_2(CO)_{10}$ with phosphines, isonitriles and pyridine under TMNO activation afforded the substitution products $Cp^*IrOs_3(\mu\text{-}H)_2(CO)_{10-n}L_n$ ($n = 1, 2$; L = $PPh_3$, $P(OMe)_3$, $^t$BuNC, CyNC or py) in good yields. For the monosubstituted derivatives, the substitution site was exclusively at an osmium atom in an axial position for L = phosphine or phosphite. Spectroscopic evidence suggested the presence of isomers in solution for the $PPh_3$ derivative. In contrast, for L = isonitrile, the ligand occupied an equatorial site. In the disubstituted derivatives, the group 15 ligands were coordinated to two different osmium atoms, one each at an axial and an equatorial site. The isomerism and fluxional behaviour of some of these clusters have also been examined.


*Keywords:* Iridium; Osmium; Ruthenium; Heteronuclear; Cluster; Phosphine; Isonitrile; Fluxional

## 1. Introduction

In the course of development of cluster chemistry, much of the focus has naturally been on homometallic clusters. As a consequence, much is now known about, for example, their ligand substituted derivatives. Thus, phosphine substitution in the archetypal homometallic cluster $Os_3(CO)_{12}$ generally leads to occupation of an equatorial site [1], which has been shown to be dictated by steric effects, while electronic effects favour occupation of an axial site by less bulky ligands such as nitriles and isonitriles [2]. This interplay of stereoelectronic effects can often lead to axial-equatorial isomerisms, as has been observed with a number of isonitrile derivatives of $M_3(CO)_{12}$ (M = Ru, Os) [3].

Heterometallic clusters, on the other hand, offer the possibility of metalloselectivity in ligand substitution and also site selectivity due to a decrease in molecular symmetry. Studies on metalloselectivity in these clusters have revealed that the selectivity could be influenced by factors such as the nature of the metals and the nature of both the existing and incoming ligands [4], but it has been observed in a number of phosphine substitutions in tetrahedral heterometallic clusters that the first substitution is always at an axial or apical position, while the second substitution could be equatorial or axial [5]. The situation can be slightly more complicated with isonitriles, as in the example with the cluster $Os_3Pt(\mu\text{-}H)_2(CO)_{10}(PCy_3)(CNCy)$, in which three isomers can be obtained, all with the isonitrile ligand on an Os vertex, but which apparently can transfer to the Pt vertex on decarbonylation [6].

For tetrahedral heterometallic clusters possessing a Cp or Cp* ligand, substitution almost always occurs at the basal metal triangle as the bulky Cp ligand would inhibit substitution at the metal centre to which it is attached. For example, both mono- and disubstituted phosphine derivatives of $CpRhRu_3(\mu\text{-}H)_2(CO)_{10}$ are known, in which substitution occurred solely at the ruthenium basal triangle, although the possibility of different relative orientations of the ligands gave rise to a number of isomers. A similar situation was observed for the Cp* analogue, although the isomeric distribution was different [7]. On the other hand, the disubstituted phosphine derivative of $CpNiOs_3(\mu\text{-}H)_3(CO)_9$ showed only one isomer in which the phosphines were bound axially to two different osmium vertices [8]. In a reflection of the smaller steric bulk of

* Corresponding author.
*E-mail address:* chmlwk@nus.edu.sg (W.K. Leong).

0022-328X/$ - see front matter © 2005 Elsevier B.V. All rights reserved.
doi:10.1016/j.jorganchem.2005.09.036

isonitriles, the solid state structure of $CpWIr_3(CO)_9(CNC_6H_3Me_2\text{-}2,6)_2$ showed that both the isonitriles were bonded to the same iridium atom [9].

We have recently found a good synthetic route to the heterometallic cluster $Cp^*IrOs_3(\mu\text{-}H)_2(CO)_{10}$, **1**, a heavier analogue of the known clusters $CpRhRu_3(\mu\text{-}H)_2(CO)_{10}$ and $Cp^*RhRu_3(\mu\text{-}H)_2(CO)_{10}$ [7]. As part of our studies on metalloselectivity in heteronuclear clusters, we began our exploration of this cluster by examining its substitution chemistry with simple two-electron donors. The result of this study is reported here.

## 2. Results and discussion

Cluster **1** was found to undergo facile substitution with $PPh_3$, $P(OMe)_3$, $^t$BuNC, CyNC or pyridine, in the presence of TMNO at ambient temperatures; no reaction occurred in the absence of TMNO. Both the mono- and disubstituted derivatives $Cp^*IrOs_3(\mu\text{-}H)_2(CO)_{10-n}L_n$ ($n = 1$, L = $PPh_3$ (**2a**) $P(OMe)_3$ (**2b**), $^t$BuNC (**2c**), CyNC (**2d**), py (**2e**); $n = 2$, L = $PPh_3$ (**3a**) $P(OMe)_3$ (**3b**), $^t$BuNC (**3c**)), were obtained except for CyNC and pyridine, for which only the monosubstituted derivatives were formed. With the exception of **2e**, which decomposed during all attempts to separate or purify it, all these clusters have been characterized spectroscopically and analytically (Tables 1 and 2). The solid-state molecular structures of all these clusters, with the exception of **2c** and **2e**, have also been established by single-crystal X-ray crystallographic studies. The ORTEP plots showing the molecular structures are shown in Figs. 1–4.

All the six clusters have the same general structure in that they comprise a tetrahedral metal core, with a carbonyl bridging one Ir–Os edge, and hydrides bridging two of the Os–Os edges; one *cis* to the bridging carbonyl and the other on the Os–Os edge diametrically opposite to it. They differ only in the number and relative dispositions of the phosphorus or isonitrile substituent. The structures of **2a** and **2b** are similar, and so are those of **3a** and **3b**. A common atomic numbering scheme, together with selected bond parameters, for all six clusters is collected in Table 3.

Among the monosubstituted derivatives, it is clear that phosphorus donor ligands tend to substitute at an axial position while the isonitrile ligand substitutes at an equatorial position; this is consistent with observations on a number of related systems [7–9]. For disubstituted derivatives, the two ligands occupy different basal osmium vertices and they are at an axial and an equatorial positions, although their position relative to the bridging carbonyl differ for phosphorus donor ligands vs isonitrile. As might be expected, the longest metal–metal bonds are those bridged by hydrides [Os(2)–Os(3) and Os(2)–Os(4)]. It is also noticeable that the longest of the Ir–Os bond lengths tend to be that *trans* to a phosphorus donor or isonitrile ligand [Ir(1)–Os(2) in **2a**, **2b**, **3a** and **3b**, and Ir(1)–Os(3) in **3c**]; this may be attributed to a *trans* effect of these ligands which are stronger σ donors than CO, on the metal–metal bond.

The carbonyl bridge is asymmetric, being closer to iridium than to osmium. This cannot be accounted for fully by a difference in the sizes of the heavy atoms; the average metal–metal bond lengths in $Ir_4(CO)_{12}$ and $Os_4(CO)_{14}$ are 2.693 and 2.825 Å [10], respectively, a difference of about 0.13 Å while the difference between Os(3)–C(13) and Ir(1)–C(13) lengths range from 0.22 to 0.45 Å. The Os–P bond lengths in **2a** and **3a** are longer than the corresponding lengths in **2b** and **3b**, respectively; this is consistent with observations that the larger cone angle of $PPh_3$[$\theta = 145°$ cf. 107° for $P(OMe)_3$] and its smaller Tolman electronic parameter ($\chi$) [2068.9 and 2079.5 $cm^{-1}$ for $PPh_3$ and $P(OMe)_3$, respectively] should both lead to lengthening of the Os–P bond [1].

The solution $^1$H NMR spectra of **2a** at 300 K consisted of four resonances in the hydride region; a doublet at $\delta$ −19.94 ppm ($^2J_{P-H} = 9.0$ Hz) and three broad singlets. On lowering the temperature to 233 K, these gave way to well-resolved resonances at $\delta$ −16.65d ($^2J_{P-H} = 9.1$ Hz), $\delta$ −17.44s, $\delta$ −19.67d ($^2J_{P-H} = 10.7$ Hz) and $\delta$ −20.01d ($^2J_{P-H} = 9.1$ Hz) ppm. Integration of the $^1$H resonances

Table 1
Infrared, MS and analytical data for the derivatives **2** and **3**

| Cluster | IR ($CH_2Cl_2$) ($cm^{-1}$) | Elemental analysis (%) Found (calculated) | MS, *m*/*z* Found (calculated for $M^+$) |
|---|---|---|---|
| **2a** | $\nu_{CO}$: 2062s, 2039sh, 2024vs, 2012sh, 1982s, 1956ms, 1767w,br, 1720w,br[a] | C, 31.33 (31.42); H, 1.98 (2.28) | 1415.8 (1414.4) |
| **2b** | $\nu_{CO}$: 2037vs, 2004s, 1987m, 1962vs, 1946m, 1713ms | C, 20.87 (20.70); H, 2.30 (2.05) | 1276.3 (1276.2) |
| **2c** | $\nu_{CO}$: 2063s, 2038sh, 2027vs, 2013sh, 1981s, 1962sh, 1754w,br<br>$\nu_{CN}$: 2176m, br | C, 23.78 (23.33); H, 2.06 (2.12); N, 0.84(1.13) | 1236.8 (1235.4) |
| **2d** | $\nu_{CO}$: 2034s, 2003vs, 1989sh, 1962s, 1947sh, 1736w,br<br>$\nu_{CN}$: 2160ms,br | C, 24.92 (24.76); H, 2.36 (2.24); N, 0.97 (1.11) | 1261.2 (1261.3) |
| **2e** | $\nu_{CO}$: 2063m, 2039s, 2021sh, 1997vs, 1967sh, 1937mw, 1727w, br | Unstable | 1231.1 (1232.0) |
| **3a** | $\nu_{CO}$: 2064s, 2041sh, 2025vs, 1986m, 1965ms, 1720w,br | C, 39.73 (39.34); H, 3.03 (2.87) | 1648.1 (1648.7) |
| **3b** | $\nu_{CO}$: 2040vs, 2015s, 1995m, 1965vs, 1718m | C, 21.29 (21.00); H, 2.62 (2.57) | 1373.6 (1372.3) |
| **3c** | $\nu_{CO}$: 2065s, 2040sh, 2028vs, 2014sh, 1982s, 1756w,br<br>$\nu_{CN}$: 2184m,br | C, 26.48 (26.06); H, 2.59 (2.73); N, 1.97 (2.17) | 1290.4 (1290.4) |

[a] KBr disk: 2059s, 2023vs, 2011sh, 1984sh, 1975vs, 1961s, 1951sh, 1935ms, 1768ms, 1727w $cm^{-1}$.

Table 2
NMR data for the derivatives **2** and **3**

| Cluster | Temperature (K) | $^1$H NMR [$\delta$/(ppm)] ($d_8$-toluene) | $^{31}$P NMR [$\delta$/(ppm)] ($C_6D_6$) |
|---|---|---|---|
| **2a** (major isomer) | 300 | ($CDCl_3$) 7.51–7.32 (m, 15H, $C_6H_5$), 2.14 (s, 15H, Cp*), −16.66 (br, 1H, OsHOs), −19.54 (br, 1H, OsHOs) | ($CDCl_3$) 0.15s |
| | 233 | ($CDCl_3$) 7.51–7.32 (m, 15H, $C_6H_5$), 2.12 (s, 15H, Cp*), −16.65 (d, 1H, OsHOs, $^2J_{PH} = 9.1$ Hz), −19.67 (d, 1H, OsHOs, $^2J_{PH} = 10.7$ Hz) | |
| **2a** (minor isomer) | 300 | ($CDCl_3$) 7.51–7.32 (m, 15H, $C_6H_5$), 2.10 (s, 15H, Cp*), −19.94 (d, 1H, OsHOs, $^2J_{PH} = 7.4$ Hz) | ($CDCl_3$) 16.26s |
| | 233 | ($CDCl_3$) 7.51–7.32 (m, 15H, $C_6H_5$), 2.07 (s, 15H, Cp*), −17.44 (s, 1H, OsHOs), −20.01 (d, 1H, OsHOs, $^2J_{PH} = 9.1$ Hz) | |
| **2b** | 300 | 3.19 (d, 9H, OMe, $^3J_{PH} = 12.4$ Hz), 1.90 (s, 15H, Cp*) | 97.36s |
| | 233 | 3.08 (d, 9H, OMe, $^3J_{PH} = 12.4$ Hz), 1.83 (s, 15H, Cp*), −17.64 (d, 1H, OsHOs, $^2J_{PH} = 9.9$ Hz), −20.33 (d, 1H, OsHOs, $^2J_{PH} = 9.9$ Hz) | |
| **2c** (major isomer) | 300 | 1.88 (s, 15H, Cp*), 0.90 (br, $^t$Bu), −20.25 (br, 1H, OsHOs) | – |
| | 253 | 1.84 (s, 15H, Cp*), 0.96 (s, 9H, $^t$Bu), −18.08 (s, 1H, OsHOs), −20.02 (s, 1H, OsHOs) | – |
| **2c** (minor isomer) | 253 | 1.81(s, 15H, Cp*), 0.86 (s, 9H, $^t$Bu), −17.24 (s, 1H, OsHOs) −20.42 (s, 1H, OsHOs) | |
| **2d** (major isomer) | 298 | 3.1 (m, br, Cy), 1.89 (s, 15H, Cp*), 1.32 (br, Cy), 0.98 (br, Cy) | – |
| | 253 | 1.83 (s, 15H, Cp*), 1.29, 0.96 (br, Cy), −17.28 (s, 1H, OsHOs) −20.45 (s, 1H, OsHOs) | – |
| **2d** (Minor isomer) | 253 | 1.85 (s, 15H, Cp*), −17.99 (s, 1H, OsHOs), −20.02 (s, 1H, OsHOs) | – |
| **2e** | 300 | ($CDCl_3$) 2.13 (s, 15H, Cp*), −14.29 (br, 2H, OsHOs) | – |
| | 203 | 1.85 (s, 15H, Cp*), −17.15(s, 1H, OsHOs), −18.12 (s, 1H, OsHOs) | |
| **3a** | 300 | 7.48–6.98 (m,30H, $C_6H_5$), 2.08 (s, 15H, Cp*), −15.71(d, 1H, OsHOs, $^2J_{PH} = 14.0$ Hz), −18.18 (dd, 1H, OsHOs, $^2J_{PH} = 8.3$ Hz, 8.3 Hz) | −11.02s, −14.94s |
| **3b** | 300 | 3.48 (d, 9H, OMe, $^2J_{PH} = 11.6$ Hz) 3.27 (d, 9H, OMe, $^2J_{PH} = 11.5$ Hz), 2.05 (s, 15H, Cp*), −17.08 (d, 1H, OsHOs, $^2J_{P-H} = 10.7$ Hz), −20.41 (dd, 1H, OsHOs, $^2J_{PH} = 10.7$ Hz, 9.9 Hz) | 118.0s, 96.6s |
| **3c** (major isomer) | 298 | 2.02 (s, 15H, Cp*), −17.90 (s, 1H, OsHOs) −20.03 (s, 1H, OsHOs) | |
| | 253 | 1.98 (s, 15H, Cp*), 1.02 (s, 9H, $^t$Bu), 0.81 (s, 9H, $^t$Bu), −17.92 (s, 1H, OsHOs), −19.27 (s, 1H, OsHOs) | – |
| **3c** (minor isomer) | 253 | 2.00 (s, 15H, Cp*), 1.08 (s, 9H, $^t$Bu), 0.86 (s, 9H, $^t$Bu), −17.80 (s,1H, OsHOs), −19.99 (s, 1H, OsHOs) | – |

supported the existence of two isomers in the ratio 1:0.14 (at 233 K) in solution. A $^{31}$P{$^1$H} NMR spectrum taken at 300 K also showed two singlets at $\delta$ 0.15 and 16.26 ppm in the same ratio 1:0.14. The existence of two isomers was further corroborated by the IR spectra recorded in dichloromethane solution and as a KBr pellet;

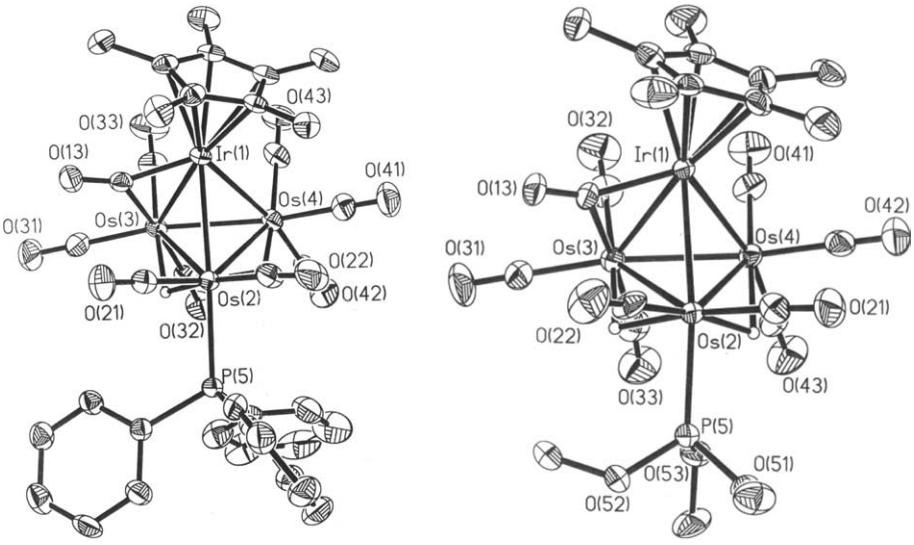


Fig. 1. ORTEP plots of **2a** (left) and **2b** (right). Thermal ellipsoids are drawn at 50% probability level. Organic hydrogens are omitted for clarity.

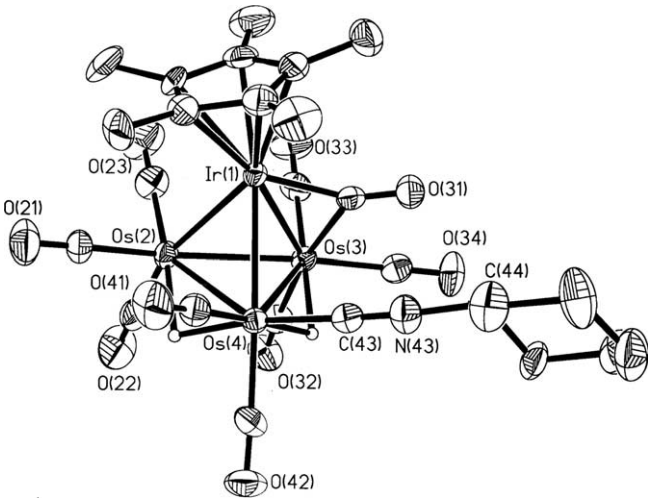


Fig. 2. ORTEP plot of **2d**. Thermal ellipsoids are drawn at 50% probability level. Organic hydrogens are omitted for clarity.

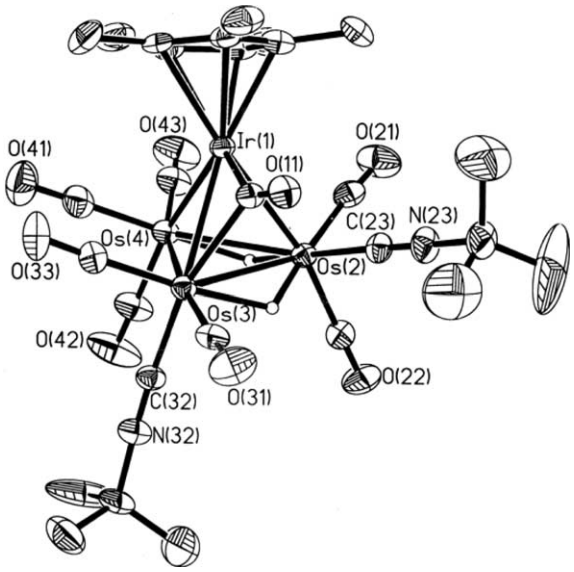


Fig. 4. ORTEP plot of **3c**. Thermal ellipsoids are drawn at 50% probability level. Organic hydrogens are omitted for clarity. Only one of the two orientations for the disordered $^t$Bu group on N(32) is shown.

both showed two broad peaks in the bridging carbonyl region, one stronger than the other. This pointed to the isomers existing in solution as well as in the solid state, and also that the bridging carbonyls persisted in solution. Thus, the two doublets at $\delta_H -16.65$d ($^2J_{P-H} = 9.1$ Hz) and $-19.67$d ($^2J_{P-H} = 10.7$ Hz), which are of equal intensity, and a Cp* signal at $\delta$ 2.14 ppm could be assigned to the major isomer, and is consistent with it having the structure obtained in the X-ray crystallographic study. It has been observed that a hydride bridging an osmium–osmium edge *cis* to a bridging carbonyl resonates at higher field than one bridging an osmium–osmium edge not *cis* to a bridging carbonyl [7,11], although a caveat here may be provided the effect of the phosphine ligand on the chemical shifts of the two hydride ligands are quite similar. In the case of the major isomer this is probably the case and so the resonance at $\delta$ $-19.67$ ppm may be assigned to the hydride bridging the Os(2)–Os(3) edge. It appears that there is a preference for axial substitution by phosphines in clusters of this general structure, even in minor isomers [7,8]. If the further assumption is made that the relative arrangements of the bridging carbonyl and hydrides remain as in all the solid-state structures obtained thus far, this arrangement being preserved also for similar derivatives of the clusters $CpRhRu_3(\mu\text{-}H)_2(CO)_{10}$ and $Cp^*RhRu_3(\mu\text{-}H)_2(CO)_{10}$ [7], then the minor isomer would correspond to substitution at either B or A′.

A $^{31}P\{^1H\}$ spin-saturation transfer experiment on **2a** performed at 300 K suggested that the two isomers were undergoing chemical exchange. The $^1H$ EXSY spectrum recorded at 273 K indicated that at that temperature, there

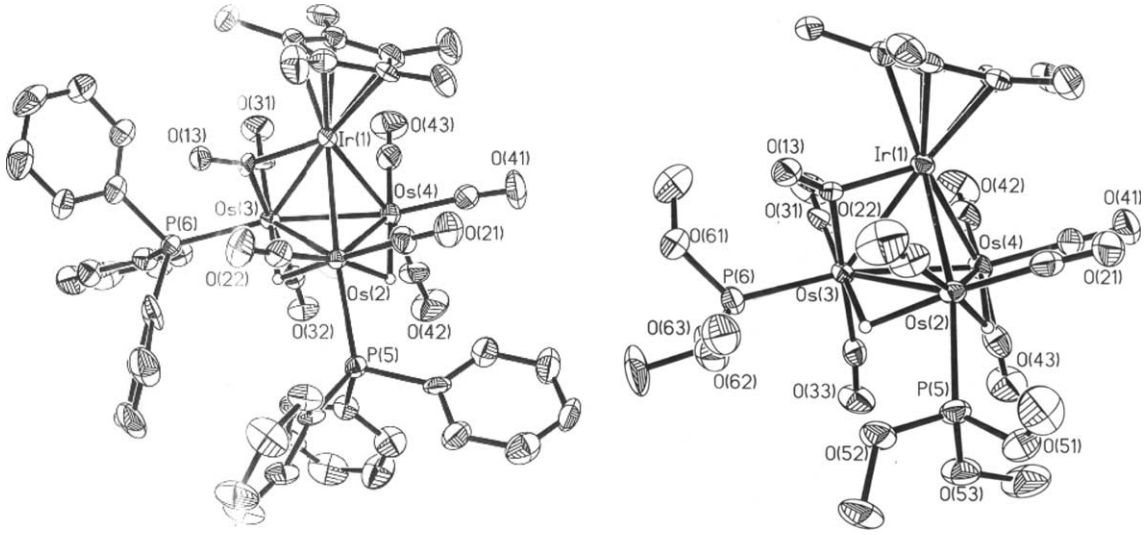


Fig. 3. ORTEP plots of **3a** (left) and **3b** (right). Thermal ellipsoids are drawn at 50% probability level. Organic hydrogens are omitted for clarity. Only one of the two orientations for each of the disordered OMe groups in **3b** is shown.

Table 3
Common atomic numbering scheme and selected bond lengths (Å) and angles (°) for the derivatives **2** and **3**

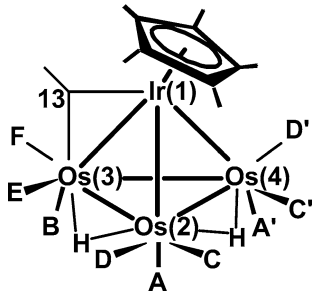


| Cluster | **2a** | **2b** | **2d** | **3a** | **3b** | **3c** |
|---|---|---|---|---|---|---|
| Ligand (L) | $PPh_3$ | $P(OMe)_3$ | CyNC | $PPh_3$ | $P(OMe)_3$ | $^t$BuNC |
| Substitution position(s)[a] | A | A | D | A,E | A,E | C,B |
| Ir(1)–Os(4) | 2.7374(3) | 2.7295(6) | 2.7303(5) | 2.7121(7) | 2.7265(3) | 2.7140(4) |
| Ir(1)–Os(3) | 2.7642(3) | 2.7768(6) | 2.7891(5) | 2.7454(7) | 2.7395(3) | 2.7917(4) |
| Ir(1)–Os(2) | 2.7909(3) | 2.7912(6) | 2.7856(5) | 2.7878(7) | 2.7861(3) | 2.7804(4) |
| Os(2)–Os(4) | 2.8822(3) | 2.8781(6) | 2.8709(5) | 2.9008(7) | 2.8757(4) | 2.8924(4) |
| Os(2)–Os(3) | 2.9772(3) | 2.9700(6) | 2.9759(5) | 3.0039(7) | 2.9789(3) | 2.9578(4) |
| Os(3)–Os(4) | 2.8003(3) | 2.8007(6) | 2.7877(5) | 2.8147(7) | 2.8087(3) | 2.7860(4) |
| Os(2)–L(1)[b] | 2.3462(13) | 2.278(3) | 1.983(10) | 2.348(3) | 2.2727(17) | 1.969(7) |
| Os(3)–L(2)[b] | – | – | – | 2.356(3) | 2.2856(18) | 1.977(7) |
| Ir(1)–C(13) | 1.888(5) | 1.923(12) | 1.897(11) | 1.903(12) | 1.936(6) | 1.899(7) |
| Os(3)–C(13) | 2.267(5) | 2.275(13) | 2.350(11) | 2.271(14) | 2.157(6) | 2.249(7) |
| O(13)–C(13)–Ir(1) | 146.6(4) | 146.6(11) | 150.5(9) | 148.4(12) | 140.2(5) | 145.9(6) |
| O(13)–C(13)–Os(3) | 130.5(4) | 131.0(10) | 128.2(8) | 129.3(11) | 136.0(5) | 130.0(5) |

[a] Positions A and B are axial; C–F are equatorial.
[b] L(1) and L(2) refers to ligand substituted at first and second positions indicated, respectively.

was only mutual chemical exchange of the hydride resonances of the major isomer, i.e., a fluxional process (Fig. 5). At room temperature, exchange crosspeaks between all the hydrides were observed, i.e., there is an additional isomerisation process. These suggest that the simple fluxional exchange within the major isomer is more facile than the isomerisation process. The former can be understood in terms of the rocking motion which has been described for the $RhRu_3$ analogues; [7] this corresponds to an incomplete merry-go-round involving the bridging carbonyl and the terminal carbonyls B, F, A′ and D′ (diagram in Table 3), which effectively moves the bridging carbonyl from the Ir(1)–Os(3) edge to the Ir(1)–Os(4) edge. For the isomerisation process, a hydride migration will also be required.

In contrast to **2a**, the NMR spectra of **2b** did not suggest the presence of isomers in solution. A similar occurrence of two isomers in solution, however, appeared for both **2c** and **2d**. The $^1$H NMR spectra of both showed two broad hydride resonances at ambient temperatures, which on lowering the temperature to 253 K, gave way to four resonances that are assignable to two isomers, in a 1:1 ratio for **2c** and a 1.0:0.3 ratio for **2d**; it was noted that the ratio for **2c** changed to 2:1 on lowering the temperature further to 203 K. Both compounds were unstable in solution, and decomposed in a few hours. The similar NMR characteristics for **2c** and **2d** suggest that the isomerism present in both is the same. Presumably, the major isomers have the structure exhibited in the solid-state structure of **2d**, *viz*., isonitrile substitution at position D. Interestingly, the $^1$H EXSY spectrum of **2c** recorded at 253 K showed only chemical exchange between the hydride resonances of the

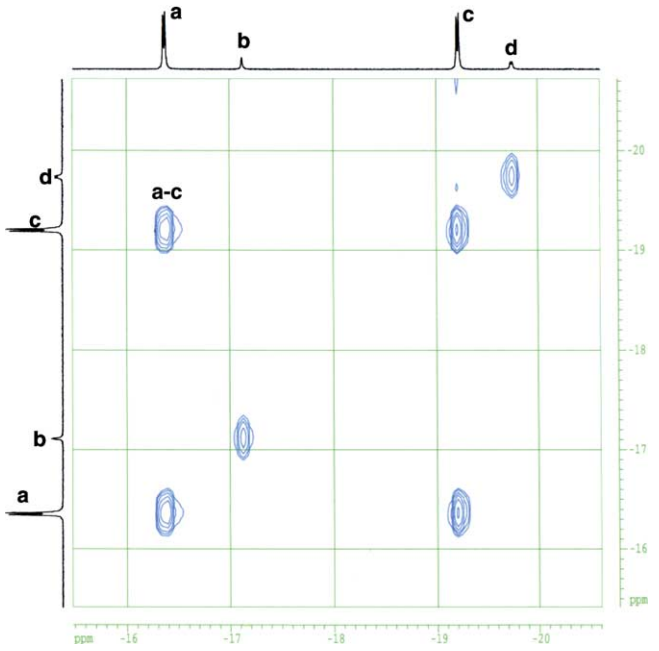


Fig. 5. $^1$H EXSY spectrum of **2a** recorded at 273 K. $\tau_m = 0.5$ s.

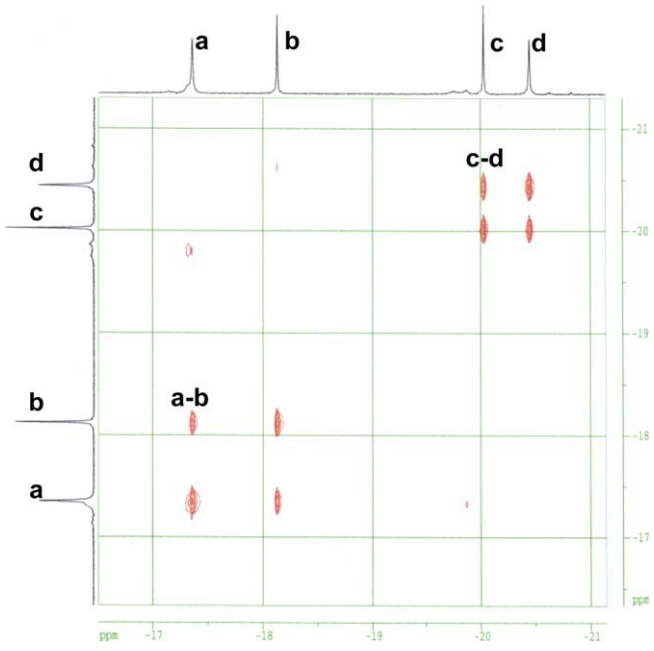


Fig. 6. $^1$H EXSY spectrum ($d_8$-toluene) of **2c** recorded at 253 K. $\tau_m = 0.1$ s.

two isomers (Fig. 6). This very specific isomerisation process (only crosspeaks corresponding to a–b and c–d exchange are observed) strongly suggests that the minor isomer corresponds to isonitrile substitution at position C; the exchange presumably involving the same mechanism mentioned above [7], the net result of which is that the bridging carbonyl is moved from bridging the Ir(1)–Os(3) edge to the Ir(1)–Os(4) edge. The hydride resonances can thus be tentatively assigned as shown in Fig. 7, but there is ambiguity in the assignment within each isomer.

Among the disubstituted derivatives in this study, only **3c** showed the presence of isomers in solution. Two pairs of hydride resonances were evident in the $^1$H NMR at 253 K, although at ambient temperature only two fast-exchange limit singlets were observed. Since the solid state structure of **3c** showed ligand substitutions at B and C, and from the foregoing discussion on **2c**, the minor isomer

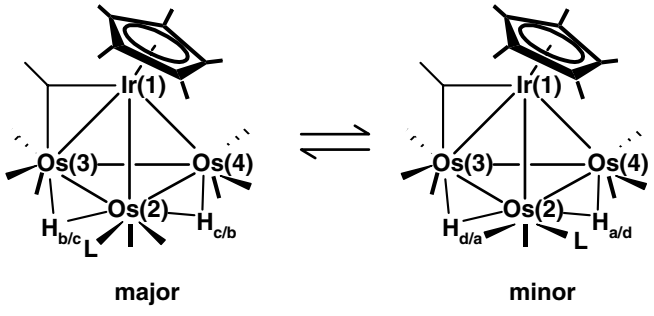


Fig. 7. Proposed structures and tentative $^1$H NMR assignments for the isomers of **2c**. L = isonitrile.

probably corresponded to substitution at A′ and D. However, a similar rocking motion to that in the monosubstituted derivatives cannot be responsible since position B (and A′) is now taken up by the isonitrile ligand; the exchange mechanism is therefore unknown.

Cluster **2e** was only characterized spectroscopically in solution as all attempts at purification resulted in decomposition. The $^1$H NMR spectrum of the crude reaction mixture recorded at room temperature showed two singlets at $\delta$ 2.11 and 2.13 ppm assignable to Cp* groups of **1** and the product, respectively. There was also a broad singlet at $\delta$ −14.29 ppm which at lower temperatures resolved into two singlets of equal intensities. A FAB-MS spectrum of the crude reaction mixture showed a very strong molecular ion cluster of peaks centered at $m/z = 1231.1$ and fragment clusters of peaks corresponding to successive loss of up to nine carbonyls, thus supporting the formulation as Cp*Ir$Os_3(\mu\text{-}H)_2(CO)_9$(py). It is noteworthy, however, that the IR spectrum of **2e** in the carbonyl stretch region had a very different pattern from those of **2a–d**, suggesting that the substitution site for pyridine is different from that of the others.

## 3. Conclusions

We have shown that the heterometallic cluster Cp*Ir$Os_3(\mu\text{-}H)_2(CO)_{10}$ undergoes facile ligand substitution reactions in the presence of TMNO to afford both mono- and disubstituted clusters. The first substitution by a phosphorus donor ligand is at an axial position while that by an isonitrile is at an equatorial position, at a basal vertex. For both sets of ligands, however, the disubstituted products have the ligands on different basal vertices, one being in an equatorial and the other in an axial position. There is clearly an inter-play of stereoelectronic effects. Some of the clusters also exhibit isomerism and fluxional behaviour.

## 4. Experimental

### 4.1. General procedures

All reactions and manipulations were carried out under nitrogen using standard Schlenk techniques. Solvents were purified, dried, distilled and stored under nitrogen prior to use. Routine NMR spectra were recorded on a BRUKER ACF-300 FT-NMR spectrometer. $^1$H chemical shifts reported are referenced against the residual proton signals of the solvents, and $^{31}$P with respect to 85% aqueous $H_3PO_4$ (external standard). Selective decoupling, spin saturation transfer and 2D spectra (EXSY, NOESY) were acquired on a Bruker Avance DRX500 or Bruker AMX500 machine. Mass spectra were obtained on a Finnigan MAT95XL-T spectrometer in an *m*-nitrobenzyl alcohol matrix. Microanalyses were carried out by the microanalytical laboratory at the National University of

Table 4
Amounts of reactants and products for the substitution reactions of **1**

| Mass of **1** used | Ligand | Amount of ligand | Product | $R_f$ | Yield |
|---|---|---|---|---|---|
| 60 mg, 0.05 mmol | $PPh_3$ | 20 mg, 0.07 mmol | **2a** | 0.30 | 50 mg, 69% |
| | | | **3a** | 0.15 | 12 mg, 14% |
| 30 mg, 0.025 mmol | $P(OMe)_3$ | 0.003 ml, 0.04 mmol | **2b** | 0.29 | 20 mg, 63% |
| | | | **3b** | 0.07 | 5.3 mg, 15% |
| 30 mg, 0.025 mmol | $^t$BuNC | 0.006 ml, 0.05 mmol | **2c** | 0.19 | 22 mg, 70% |
| | | | **3c** | 0.11 | 6 mg, 17% |
| 30 mg, 0.025 mmol | CyNC | 0.004 ml, 0.03 mmol | **2d** | 0.25 | 24 mg, 75% |

Singapore. The cluster **1** was prepared according to the published method [12]. All other reagents were from commercial sources and used as supplied.

### 4.2. Reaction of *1* with triphenyl phosphine

To a 250 ml three-necked flask containing **1** (60 mg, 0.051 mmol) in dichloromethane (10 ml) was added $PPh_3$ (20 mg, 0.076 mmol). A solution of trimethylamine *N*-oxide (6.7 mg, 0.07 mmol) in deoxygenated dichloromethane (20 ml) was introduced dropwise into the solution of **1** via a pressure equalizing dropping funnel over a period of 2 h. The solution was stirred for a further 1 h. Removal of the solvent by rotary evaporation followed by chromatographic separation (6:4, v/v, hex/dcm) on silica gel TLC plates yielded a red band of $Cp^*IrOs_3(H)_2(CO)_9(PPh_3)$, **2a**, and another red band of $Cp^*IrOs_3(H)_2(CO)_8(PPh_3)_2$, **3a**. A similar procedure was employed with the other ligands, as summarized in Table 4.

### 4.3. X-ray crystal structure determinations

Crystals were grown from dichloromethane/hexane solutions and mounted on quartz fibres. X-ray data were collected on a Bruker AXS APEX system, using Mo Kα radiation, at 223 K with the SMART suite of programs [13]. Data were processed and corrected for Lorentz and polarisation effects with SAINT [14], and for absorption effects with SADABS [15]. Structural solution and refinement were carried out with the SHELXTL suite of programs [16]. Crystal and refinement data are summarised in Tables 5 and 6.

The structures were solved by direct methods to locate the heavy atoms, followed by difference maps for the light, non-hydrogen atoms. All non-hydrogen atoms were generally given anisotropic displacement parameters in the final model. Organic hydrogen atoms were placed in calculated positions and refined with a riding model. The metal hydrides in **2a**, **3b** and **3c** were located in low angle difference maps, while those in **2b**, **2d** and **3a** were placed in calculated positions using XHYDEX [17]. There were disorder of two of the OMe groups in **3b**, and of one of the $^t$Bu groups in **3c**; each were modeled with two alternative positions and appropriate restraints placed.

## Acknowledgments

This work was supported by the National University of Singapore (Research Grant No. R143-000-149-112) and one of us (P.S.) thanks the University for a Research Scholarship.

Table 5
Crystal and refinement data for **2a**, **2b** and **2d**

| Compound | **2a** | **2b** | **2d** |
|---|---|---|---|
| Empirical formula | $C_{37}H_{32}IrO_9Os_3P$ | $C_{22}H_{26}IrO_{12}Os_3P$ | $C_{26}H_{28}IrNO_9Os_3$ |
| Formula weight | 1414.40 | 1276.20 | 1261.29 |
| Crystal system | Triclinic | Monoclinic | Monoclinic |
| Space group | $P\bar{1}$ | $P2_1/c$ | $P2_1/c$ |
| $a$ (Å) | 10.0041(3) | 18.4173(18) | 9.8674(6) |
| $b$ (Å) | 13.7645(5) | 9.7730(9) | 10.9098(6) |
| $c$ (Å) | 14.5798(5) | 18.6227(18) | 14.3200(8) |
| $\alpha$ (°) | 78.676(1) | 90 | 90 |
| $\beta$ (°) | 86.286(1) | 117.830(2) | 102.908(1) |
| $\gamma$ (°) | 70.749(1) | 90 | 90 |
| $V$ (Å$^3$) | 1858.50(11) | 2964.2(5) | 1502.61(15) |
| $Z$ | 2 | 4 | 2 |
| $\rho_{calc}$ (Mg/m$^3$) | 2.527 | 2.860 | 2.788 |
| Absorption coefficient (mm$^{-1}$) | 13.887 | 17.403 | 17.107 |
| $F(000)$ | 1292 | 2296 | 1136 |
| Crystal size (mm$^3$) | $0.12 \times 0.06 \times 0.06$ | $0.36 \times 0.20 \times 0.06$ | $0.33 \times 0.15 \times 0.07$ |
| $\theta$ Range for data collection (°) | 2.16–29.43 | 2.19–26.37 | 2.29–30.01 |
| Reflections collected | 25 504 | 26 985 | 13 889 |
| Independent reflections ($R_{int}$) | 9246 (0.0338) | 6057 (0.0658) | 8297 (0.0400) |
| Data/restraints/parameters | 9246/0/473 | 6057/0/360 | 8297/1/366 |
| Goodness-of-fit on $F^2$ | 0.994 | 1.058 | 1.005 |
| Final $R$ indices [$I > 2\sigma(I)$] | $R_1 = 0.0289$, $wR_2 = 0.0640$ | $R_1 = 0.0488$, $wR_2 = 0.1152$ | $R_1 = 0.0376$, $wR_2 = 0.0779$ |
| $R$ indices (all data) | $R_1 = 0.0407$, $wR_2 = 0.0672$ | $R_1 = 0.0580$, $wR_2 = 0.1207$ | $R_1 = 0.0416$, $wR_2 = 0.0798$ |
| Largest difference in peak and hole (e Å$^{-3}$) | 1.962 and −0.794 | 3.695 and −2.654 | 2.221 and −1.522 |

Table 6
Crystal and refinement data for **3a–c**

| Compound | **3a** | **3b** | **3c** |
|---|---|---|---|
| Empirical formula | $C_{54}H_{47}IrO_8Os_3P_2$ | $C_{24}H_{35}IrO_{14}Os_3P_2$ | $C_{28}H_{35}IrN_2O_8Os_3$ |
| Formula weight | 1648.66 | 1372.26 | 1290.38 |
| Crystal system | Triclinic | Monoclinic | Triclinic |
| Space group | $P\bar{1}$ | $P2_1/c$ | $P\bar{1}$ |
| $a$ (Å) | 13.0331(9) | 17.9642(7) | 9.9572(6) |
| $b$ (Å) | 13.0913(9) | 9.4765(3) | 11.2613(6) |
| $c$ (Å) | 17.4377(12) | 20.2004(7) | 16.3334(9) |
| $\alpha$ (°) | 105.049(2) | 90 | 76.2690(10) |
| $\beta$ (°) | 92.577(2) | 95.172(1) | 83.7040(10) |
| $\gamma$ (°) | 110.219(2) | 90 | 73.6600(10) |
| $V$ (Å$^3$) | 2666.2(3) | 3424.9(2) | 1705.47(17) |
| $Z$ | 2 | 4 | 2 |
| $\rho_{calc}$ (Mg/m$^3$) | 2.054 | 2.661 | 2.513 |
| Absorption coefficient (mm$^{-1}$) | 9.724 | 15.121 | 15.074 |
| $F(000)$ | 1540 | 2504 | 1172 |
| Crystal size (mm$^3$) | $0.16 \times 0.08 \times 0.03$ | $0.18 \times 0.13 \times 0.05$ | $0.15 \times 0.09 \times 0.08$ |
| $\theta$ Range for data collection (°) | 2.13–26.37 | 2.02–30.02 | 2.07–26.37 |
| Reflections collected | 35856 | 49890 | 23064 |
| Independent reflections ($R_{int}$) | 10904 (0.0671) | 9439 (0.0542) | 6972 (0.0331) |
| Data/restraints/parameters | 10904/11/618 | 9439/7/421 | 6972/21/403 |
| Goodness-of-fit on $F^2$ | 1.106 | 1.096 | 1.030 |
| Final $R$ indices [$I > 2\sigma(I)$] | $R_1 = 0.0600$, $wR_2 = 0.1386$ | $R_1 = 0.0384$, $wR_2 = 0.0732$ | $R_1 = 0.0301$, $wR_2 = 0.0636$ |
| $R$ indices (all data) | $R_1 = 0.0754$, $wR_2 = 0.1469$ | $R_1 = 0.0499$, $wR_2 = 0.0771$ | $R_1 = 0.0409$, $wR_2 = 0.0671$ |
| Largest difference in peak and hole (e Å$^{-3}$) | 5.755 and −1.686 | 1.854 and −0.966 | 1.456 and −0.762 |

## Appendix A. Supplementary data

Crystallographic data (excluding structure factors) for the structures in this paper have been deposited with the Cambridge Crystallographic Data Centre as supplementary publication numbers CCDC 281005–281010. Copies of the data can be obtained, free of charge, on application to CCDC, 12 Union Road, Cambridge CB2 1EZ, UK, (fax: +44 1223 336 033 or e-mail: deposit@ccdc.cam.ac.uk). Supplementary data associated with this article can be found, in the online version, at doi:10.1016/j.jorganchem.2005.09.036.

## References

[1] (a) For example: K. Biradha, V.M. Hansen, W.K. Leong, R.K. Pomeroy, M.J. Zaworotko, J. Cluster Sci. 11 (2000) 285;
(b) M.I. Bruce, M.J. Liddell, C.A. Hughes, B.W. Skelton, A.H. White, J. Organomet. Chem. 347 (1988) 157;
(c) M.I. Bruce, M.J. Liddell, C.A. Hughes, J.M. Patrick, B.W. Skelton, A.H. White, J. Organomet. Chem. 347 (1988) 181.
[2] (a) P.J. Dyson, J.S. McIndoe, Transition Metal Carbonyl Cluster Chemistry, Gordon & Breach, Australia, 2000;
(b) R.F. Alex, F.W.B. Einstein, R.H. Jones, R.K. Pomeroy, Inorg. Chem. 26 (1987) 3175;
(c) M.R. Churchill, B.G. DeBoer, Inorg. Chem. 16 (1977) 2397;
(d) T. Venalainen, T. Pakkanen, J. Organomet. Chem. 266 (1984) 269;
(e) M.I. Bruce, J.G. Matisons, B.W. Skelton, A.H. White, J. Chem. Soc., Dalton Trans. (1983) 2375;
(f) B.F.G. Johnson, J. Lewis, B.E. Reichert, K.T. Schorpp, J. Chem. Soc., Dalton Trans. (1976) 1403;
(g) D.J. Dahm, R.A. Jacobson, J. Am. Chem. Soc. 90 (1968) 5106.
[3] (a) G. Chen, W.K. Leong, J. Organomet. Chem. 574 (1999) 276;
(b) M.I. Bruce, G.N. Pain, C.A. Hughes, J.M. Patrick, B.W. Skelton, A.H. White, J. Organomet. Chem. 307 (1986) 343;
(c) M.J. Mays, P.D. Gavens, J. Chem. Soc., Dalton Trans. (1980) 911;
(d) R.D. Adams, N.M. Golembeski, Inorg. Chem. 18 (1979) 1909;
(e) R.D. Adams, N.M. Golembeski, J. Am. Chem. Soc. 101 (1979) 2579.
[4] (a) For example: A.U. Harkonen, M. Ahlgren, T.A. Pakkanen, J. Pursiainen, Organometallics 16 (1997) 689;
(b) P. Braunstein, J. Rose, D. Toussaint, S. Jaaskelainen, M. Ahlgren, T.A. Pakkanen, J. Pursiainen, L. Toupet, D. Grandjean, Organometallics 13 (1994) 2472;
(c) P. Braunstein, L. Mourey, J. Rose, P. Granger, T. Richert, F. Balegroune, D. Grandjean, Organometallics 11 (1992) 2628;
(d) P. Braunstein, J. Rose, P. Granger, J. Raya, S.E. Bouaoud, D. Grandjean, Organometallics 10 (1991) 3686;
(e) J. Pursiainen, M. Ahlgren, T.A. Pakkanen, J. Valkonen, J. Chem. Soc., Dalton Trans. (1990) 1147;
(f) J. Pursiainen, T.A. Pakkanen, J. Jaaskelainen, J. Organomet. Chem. 290 (1985) 85.
[5] (a) G. Süss-Fink, S. Haak, V. Ferrand, A. Neels, H. Stoeckli-Evans, J. Organomet. Chem. 580 (1999) 225;
(b) H. Matsuzaka, T. Kodama, Y. Uchida, M. Hidai, Organometallics 7 (1988) 1608;
(c) B.F.G. Johnson, J. Lewis, P.R. Raithby, S.N. Azman, B. Syed-Mustaffa, M.J. Taylor, K.H. Whitmire, W. Clegg, J. Chem. Soc., Dalton Trans. (1984) 2111;
(d) J.R. Fox, W.L. Gladfelter, T.G. Wood, J.A. Smegal, T.K. Foreman, G.L. Geoffroy, I. Tavaniepour, V.W. Day, C.S. Day, Inorg. Chem. 20 (1981) 3214.
[6] P. Ewing, L. Farrugia, J. Organomet. Chem. 7 (1988) 871.
[7] (a) J.L. Le Grand, W.E. Lindsell, K.J. McCullough, J. Organomet. Chem. 413 (1991) 321;
(b) W.E. Lindsell, N.M. Walker, A.S.F. Boyd, J. Chem. Soc., Dalton Trans. (1988) 675.
[8] E. Sappa, M.L.N. Marchino, G. Predieri, A. Tiripicchio, M.T. Camellini, J. Organomet. Chem. 307 (1986) 97.

[9] S.M. Waterman, M.G. Humphrey, D.C.R. Hockless, J. Organomet. Chem. 579 (1999) 75.
[10] (a) M.R. Churchill, J.P. Hutchinson, Inorg. Chem. 17 (1978) 3528; (b) V.J. Johnston, F.W.B. Einstein, R.K. Pomeroy, Organometallics 7 (1988) 1867.
[11] M.R. Churchill, C. Bueno, S. Kennedy, J.C. Bricker, J.S. Plotkin, S.G. Shore, Inorg. Chem. 21 (1982) 627, and references therein.
[12] P. Srinivasan, W.K. Leong, J. Organomet. Chem., in press.
[13] SMART, version 5.628, Bruker AXS Inc., Madison, WI, USA, 2001.
[14] SAINT+, version 6.22a, Bruker AXS Inc., Madison, WI, USA, 2001.
[15] G.M. Sheldrick, SADABS, 1996.
[16] SHELXTL, version 5.1, Bruker AXS Inc., Madison, WI, USA, 1997.
[17] A.G. Orpen, XHYDEX: A Program for Locating Hydrides in Metal Complexes, School of Chemistry, University of Bristol, UK, 1997.